ORIGINAL ARTICLE

Oxygen-Permeable Films for Continuous Additive, Subtractive, and Hybrid Additive/Subtractive Manufacturing

Puskal Kunwar, Zheng Xiong, Shannon Theresa Mcloughlin, and Pranav Soman

Abstract

In the past 5 years, oxygen-permeable films have been widely used for continuous additive manufacturing. These films create a polymerization inhibition zone that facilitates continuous printing in the additive mode of fabrication. Typically, oxygen-permeable films made out of Teflon are currently used. These films are expensive and are not commonly available. Hence, this research work investigates the feasibility of using commonly available low-cost oxygen-permeable films made from polydimethylsiloxane (PDMS) and polyurethane for continuous additive manufacturing. We also characterize the ablation depth range that can be achieved using these films and the potential use for subtractive ablation-based manufacturing as well as hybrid additive/subtractive manufacturing. Results demonstrate that the PDMS films ($600\,\mu m$ thick) can be used for both additive and subtractive modes, whereas spin-coated PDMS thin film ($40\,\mu m$ thick) on glass coverslip and breathe-easy polyurethane film ($20\,\mu m$ thick) laminated on glass coverslip are suitable only for additive mode of fabrication. The latter two films are oxygen impermeable, however, they retain oxygen, which is capable of creating dead zone and thereby facilitates continuous printing. We anticipate that this work will help researchers to choose the appropriate oxygen-permeable film for continuous additive, subtractive, and hybrid additive/subtractive manufacturing of complex three-dimensional structures for a range of applications.

Keywords: dead zone, ablation z-range, hydrogel, oxygen-permeable films, hybrid laser printing, subtractive printing

Introduction

NEXT-GENERATION MICROFLUIDICS, soft robotics, flexible electronics, and organ-on-a-chip applications require new capabilities to manufacture high-resolution multiscale structures using soft polymer and hydrogel materials.[1–3] Current fabrication methods based on additive and/or subtractive approaches are limited in their ability to print complex multiscale three-dimensional (3D) constructs and devices using soft materials.[4–7] Subtractive manufacturing methods such as soft lithography, nanoimprint lithography, electron-beam etching, and ion beam milling lithography can provide high-resolution multiscale features, however, the fabrication is mostly limited for developing two-dimensional devices.[8–10] Advanced techniques such as multiphoton ablation (MPA) can sculpt 3D features within soft materials, however, limited processing depth and low scalability/throughput make this method unfeasible for making functional devices.[11] Printing complex 3D structures is possible with additive methods based on extrusion-based fused deposition modeling and light-based digital projection lithography, but the resolution of these methods is typically limited to $\sim 50\,\mu m$ or lower.[12–14] Multiphoton polymerization (MPP) is capable of printing 3D structures using soft materials with nano-to-micrometer resolution, yet low scalability makes this process unfeasible for making centimeter-scale constructs.[15,16]

Newer advancement in additive manufacturing techniques such as continuous liquid interphase printing (CLIP) enables high-resolution printing in a quick and continuous manner.[17] This is achieved by generating a continuous liquid interface of uncured resin between the crosslinking part and a fabrication window made out of oxygen-permeable Teflon thin films. However, printing 3D structures with internal hollow structures below $25\,\mu m$ sizes is not possible with this approach.[17] A new technology coined as Hybrid Laser Printing (HLP) is demonstrated that synergistically combines additive CLIP, additive MPP, and subtractive MPA approaches.[18] HLP is capable of printing technically challenging 3D structures with

Department of Biomedical and Chemical Engineering, Syracuse University, Syracuse, New York, USA.

embedded channels, overhangs, and undercuts with a minimum resolution of ∼3 μm. HLP utilizes an oxygen-permeable Teflon film as the fabrication window to facilitate continuous and quick printing during the additive and subtractive modes of fabrication.

Detailed characterization of the oxygen-permeable film is critical for additive CLIP, subtractive ablation-based, and hybrid HLP technologies. In this report, we characterize the properties of commonly available low-cost films made from polydimethylsiloxane (PDMS) and polyurethane, as an alternative to the expensive and exclusive Teflon films. Dead zone thickness and achievable crosslinked layer thickness for poly (ethylene glycol) diacrylate (PEGDA) hydrogel were characterized for a different laser dose, a function of exposure time, and laser power for all films. Furthermore, ablation z-range was characterized for all the films. We also assessed the suitability of various films to achieve high fabrication speeds and superior resolution during additive and additive/subtractive modes. We also demonstrate the fabrication of one exemplary structure using each of these thin films.

Materials and Methods

Oxygen-permeable films

Teflon films are exclusive to few vendors who charge several hundred dollars even for a single film of size $12 \times 12 \times 0.045 \, mm^3$. We compared four different oxygen-permeable films for additive and additive/subtractive modes. (a) Teflon film. Teflon film (AF-2400 X) with a nominal thickness of 45 μm was bought from Biogeneral, Inc. and directly used without any modification. (b) PDMS films. PDMS solution was prepared by mixing Sylgard 184 silicone elastomer base and curing agent (10:1) and was degassed in a desiccator to remove air bubbles. The 600-μm-thin PDMS film was prepared using a mold and is referred to as PDMS-1. The thickness of the Teflon film used in the previous studies ranged from 45 to 100 μm, and hence, we chose the Teflon with same thickness; however, using PDMS as the oxygen-permeable film of similar thickness, due to its low flexure rigidity, the polymer solution flexed the film down, and hence, we used a relatively thick PDMS film of 600 μm. (c) The spin-coated PDMS thin film was prepared by spin coating the degassed PDMS solution at a speed of 1500 rpm for 2 min onto the glass coverslip of 150 μm, resulting in a PDMS film of 40 μm. This film is referred to as PDMS-2 (d) polyurethane breathe-easy film. A 20 μm thin breath-easy film (Sigma-Aldrich) was laminated on a similar glass coverslip of 150 μm thickness (18 × 18 mm, no.1; Globe Scientific). Since this is made out of polyurethane, this is referred to as PU in this work. These films are chosen as they are inexpensive and easily available.

Additive/subtractive fabrication setup

To character the oxygen-permeable films, we built an optical fabrication setup that is able to continuously print a 3D structure in both additive and subtractive modes of fabrication. The additive mode uses a 350–450 nm laser beam obtained by passing a femtosecond (fs) laser (700–900 nm) through a second-harmonic generator (Fig. 1a). This beam, spatially modulated by a digital micromirror device (DMD), can polymerize features as large as $1 \, cm^2$ with a resolution of 30 μm. The subtractive mode utilizes an fs laser to either crosslink a structure using two-photon polymerization or ablate features within previously crosslinked structures using two-photon ablation. The sample holder assembly consists of the L-shaped stage and a plastic Petri dish with a hole bored in the middle, and an oxygen- permeable, UV-transparent, and chemically inert film is glued over the hole forming a fabrication window. The film creates a polymerization inhibition zone, known as dead zone due to oxygen diffusion through the film, as shown in Figure 1b. Formation of dead zone prevents the adhesion of newly crosslinked layers to the fabrication window and allows continuous drawing-in of liquid hydrogel prepolymer solution. The light absorption and scattering properties of the film and prepolymer solution also determine an optimal ''ablation z-range''; in this range,
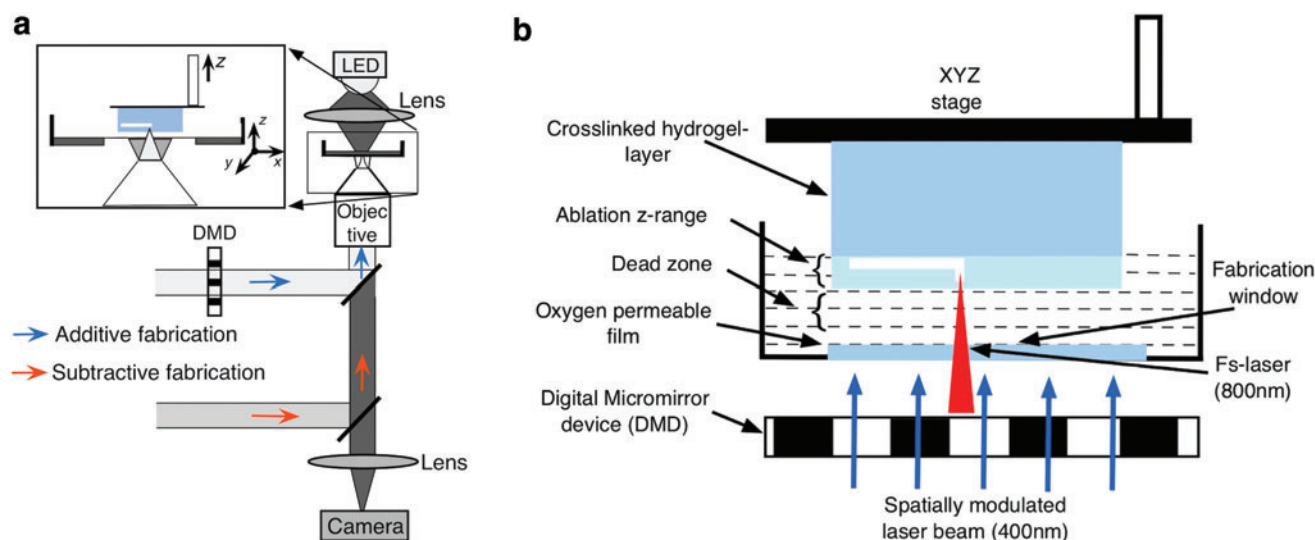

FIG. 1. (a) Schematic diagram of hybrid laser printing setup. (b) Schematic showing the sample holder assembly and stage. Key parameters such as dead zone and ''ablation z-range'' for the hybrid laser printer are also illustrated. Color images are available online.

the material can be machined without any unwanted effects such as incomplete removal or bubble formation (Fig. 1b).

To fabricate structures using the optical setup shown in Figure 1, a 3D model of a structure is sliced into several layers, converted to virtual digital masks, and uploaded to a DMD, where individual micromirrors can be switched into either an ON state or an OFF state based on the virtual masks. Light modulated by the DMD is used for selective cross-linking of PEGDA prepolymer. The changes in the mask exposure are synchronized to the Z-movement of the L-shaped stage to print a 3D structure in a continuous layer-by-layer manner. The fs laser is then utilized to ablate hollow features and channels at micrometer resolution based on the design. An iteration of sequential additive and subtractive processes fabricates a complete multiscale 3D structure.

Hydrogel solution preparation

For the experiments, we prepared a prepolymer solution consisting of 30% poly (ethylene glycol) diacrylate (PEGDA, Mw = 700; Sigma-Aldrich) with 1% lithium phenyl-2,4,6-trimethylbenzoylphosphinate (LAP). LAP was synthesized in a laboratory using a previously mentioned protocol.[19] First, 0.3 g of LAP were added to 21 mL of Millipore water and mixed thoroughly using the Vortex mixer (Vortex-Genie 2; Fisher Scientific). Subsequently, 9 mL of PEGDA solution were added to the LAP solution, further mixed in the Vortex mixer, and stored at 37°C.

Transmission spectra measurement

The optical transparency of the oxygen-permeable films was studied by measuring the transmission spectra using evolution 201/202 spectrophotometers (Thermo Fisher).

Dead zone measurement

To measure the dead zone thickness, the stage was placed exactly at $200 \mu m$ from the upper surface of the oxygen-permeable film as the dead zone of the thin film is mostly around 20 to $100 \mu m$. A spatially modulated laser beam was exposed to crosslink a uniform square-shaped structure. The thickness of the structure was measured using HIROX microscopy and was subtracted from $200 \mu m$ to obtain the correct dead zone thickness.

Results

Figure 2 shows the optical transmittance of Teflon, PDMS-1, PDMS-2, and PU in the wavelength range of 300–1000 nm. Based on these results, the transmittance at 400 nm (desired laser wavelength for additive crosslinking) is greater than 85% for all the films except the PU film, which is around 65%. Similarly, above 85% of light of wavelength 800 nm (desired laser wavelength for subtractive ablation) transmits through the Teflon, PDMS-1, and PDMS-2 films, whereas only about 70% of light at the same wavelength passes through the PU film. Next, the dead zone thickness was measured for all the different oxygen-permeable films. Figure 3a and b shows the plot of thickness of dead zone for all four films for different crosslinking laser powers (50, 100, 150, and 200 mW) and exposure times (5, 10, 15, and 20 s). For the laser dosages used in this work, the dead zone thickness ranges from 8 to $97 \mu m$ for Teflon and from 48 to $151 \mu m$ for
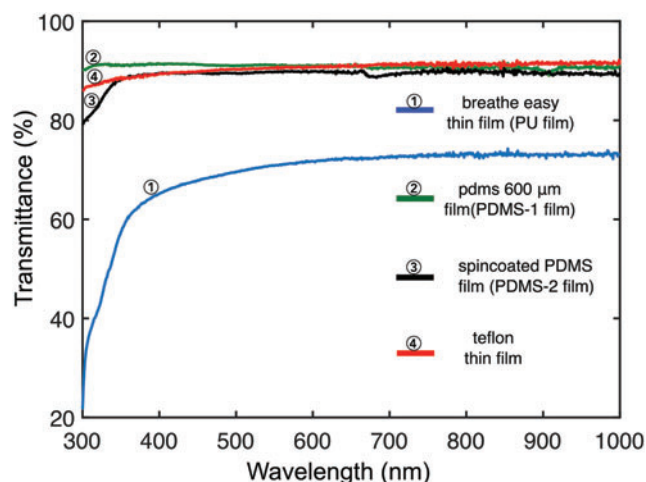

FIG. 2. Transmission spectra of oxygen-permeable films in the wavelength range of 300–1000 nm. Color images are available online.

PDMS-1 film. Furthermore, plots in both cases show a decreasing trend of dead zone thickness with increasing laser dose. As mentioned earlier, dead zone thickness has been studied using the Teflon film in a previous study.[17,18] In the previous study, dead zone thickness was measured for different laser intensities by varying the gas (nitrogen, oxygen, and air) below the fabrication window (100-μm-thick Teflon membrane). In the study, the dead zone thickness increases when pure oxygen was used below the window compared with that of air. When air was used, the dead zone thickness in the range of 20 to $80 \mu m$ is reported, which is comparable with our result. In this report, we also compare the dead zone thicknesses of PDMS-2 and PU films with the commonly used Teflon films.

We found that the dead zone was also formed for the PDMS-2 film and PU film. The dead zone for these films was obtained for different crosslinking laser powers and exposure times, as mentioned above. As shown in Figure 3c and d, the maximum dead zone thickness obtained for the PDMS-2 film is $114 \mu m$ and follows the trend of decreasing dead zone thickness with increasing laser dose. A similar trend is also observed for the PU film; however, the maximum thickness of dead zone for this film is $45 \mu m$. The glass coverslip, which acts as a base substrate for these two films, is not oxygen permeable; however, a dead zone is formed in both cases (Fig. 3c, d). We suggest that the dead zone in these cases is due to the presence of absorbed oxygen retained by these films. In both cases, the prepolymer hydrogel solution is needed to be removed from the sample holder after each fabrication so that the film is exposed to air, otherwise, the crosslinked structures stick to the film. Furthermore, we studied the speed of additive fabrication for all the films. Structures were readily printed using PDMS-1, PDMS-2, and Teflon films as fabrication window with a speed of 1.44 m/h and this was the highest speed achievable by our motorized stage. This result is comparable with the speed of fabrication obtained using Teflon film in our previous work,[18] and the work by another research group.[17] With even a small dead zone thickness for PU films, a fabrication speed of 0.7 m/h was achieved. Figure 3e and f shows the Empire State Building structure fabricated using the PU film with a speed
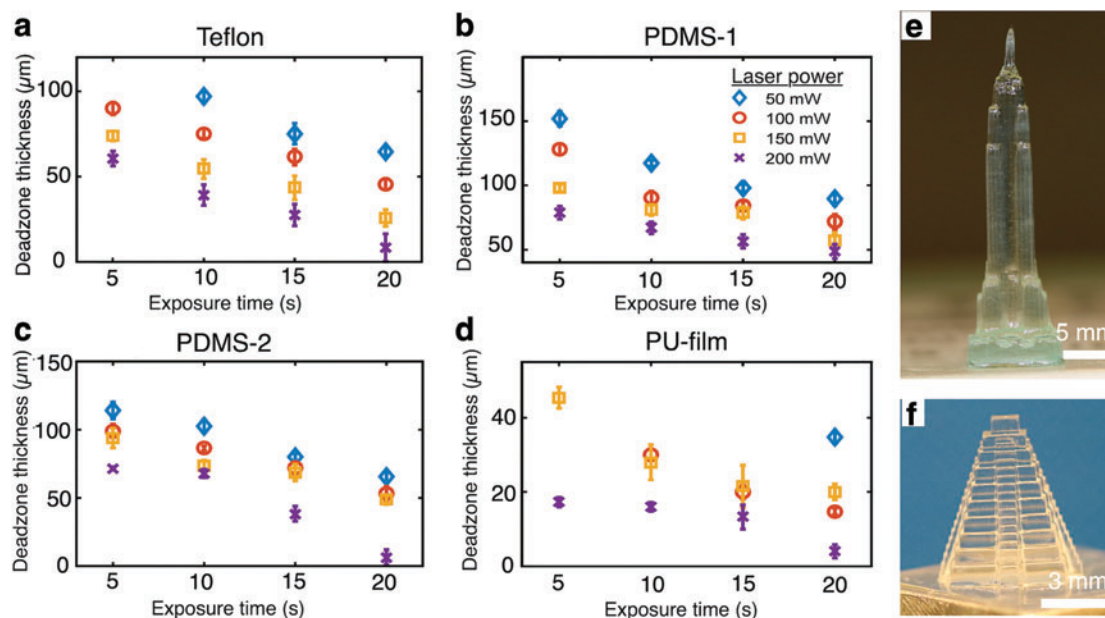
FIG. 3. **(a–d)** Plots showing the dead zone thickness for varying laser powers and exposure times for different films. **(e)** Empire State Building printed with the laser power of 200 mW and printing speed of 0.7 m/h using PU film and **(f)** Mayan pyramid. Color images are available online.

of 0.7 m/h, and the Mayan pyramid fabricated with a speed of 1 m/h using the PDMS-2 film.

In the subtractive mode of fabrication, material removal occurs within previously crosslinked layers restricted in a range known as "ablation z-range" and the material removal is only feasible within this range. Operating in this z-range ensures that the ablating laser beam never comes in contact with the liquid resin that prevents unwanted crosslinking and bubble formation. A detailed characterization of dead zone and "ablation z-range" is necessary to obtain the exact location of ablation and predictable sizes of ablated channels. Therefore, we have characterized the "ablation z-range" for all the four films. Based on the absorption maximum of the LAP photoinitiator, a wavelength of $\lambda = 800$ nm was chosen to induce two-photon ablation during the subtractive mode of fabrication. Furthermore, a scanning speed of 25 μm/s and an ablation laser power of 1300 mW were chosen for ablation, and direct laser ablation was performed at different depths of the crosslinked structure (crosslinking laser power of 200 mW and exposure time of 20 s).

In the case of PDMS-1 film, the thickness of dead zone was 40 μm for the crosslinking laser power of 200 mW and exposure time of 20 s. While for the chosen ablation laser power and scanning speed, the maximum ablation z-depth was 70 μm, giving an "ablation z-range" of $\sim$40–70 μm (Fig. 4a). While the "ablation z-range" for the Teflon film was $\sim$30–80 μm. Furthermore, the "ablation z-range" for the PDMS-2 and PU films was also estimated, and the z-range for the PDMS-2 film was $\sim$20–40 μm and for the PU film was $\sim$20–30 μm. It is seen from Figure 4a that the ablation z-range is small for these two films. This is because there are more interfaces (air/glass, glass/film, film/uncrosslinked hydrogel, uncrosslinked hydrogel/crosslinked hydrogel) in these film constructs compared with the first two films that induce scattering and distortion in the laser focus, thereby

limiting the penetration depth into the previously crosslinked hydrogel. Previously, work with two-photon ablation has demonstrated that 3D structures can be sculpted few hundred micrometers within hydrogels with a resolution range of 1.5–5 μm, depending upon the material.[20] Our result suggests that the structure can be ablated with the smallest feature size of $\sim$2 μm, with a laser power of 1300 mW and scanning speed of 25 μm/s, using all four films. Based on our results, the PDMS-2 thin film and PU film are mostly suitable for the additive mode of fabrication. However, the PDMS-1 film is applicable for both additive and subtractive modes of fabrication, which is equivalent to Teflon film.

Next, we demonstrate the fabrication of the complex structure that requires both additive and subtractive modes of fabrication using PDMS-1 film (Fig. 4b). We used the 600 μm PDMS film as a fabrication window to print four-well interconnected microfluidic chips using additive DMD-based printing and subtractive MPA. This chip consists of three different pairs of ablated channels printed on different Z-heights and XY locations, as shown in Figure 4b. This structure is technically challenging to print, and/or extremely time-consuming to fabricate, and/or requires complicated multiple bonding and stacking steps to fabricate this device using conventional fabrication technologies. The four-well construct shown in Figure 4b was fabricated using additive crosslinking steps that used a laser power of 200 mW and exposure time of 15 s. The subtractive MPA steps were used to print a pair of straight channels (Fig. 4b1), sawtooth (Fig. 4b2) channels, and spiral channels (Fig. 4b3) with a laser power of 1300 mW and scanning speed of 25 μm/s, using an objective lens (20$\times$; Zeiss) with numerical aperture of 0.25. Each structure is $\sim$5 μm thick and printed at different z-levels/heights at an interval of 200 μm. These channels are visualized by focusing the microscope to each embedded 3D channel structure in different z-planes as
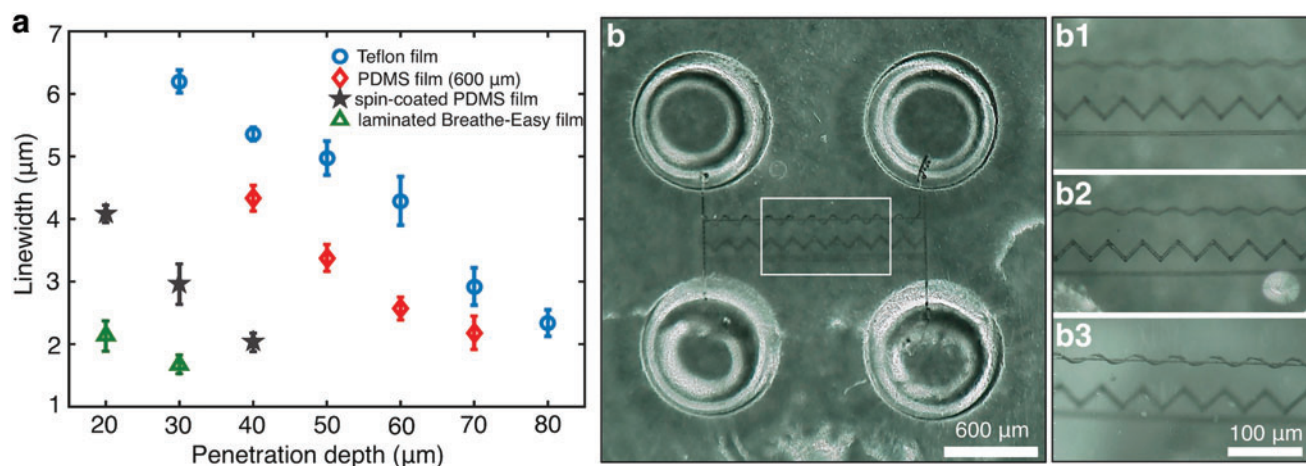
FIG. 4. **(a)** Plot depicting the ''ablation z-range'' of different oxygen-permeable films. **(b)** *Top view* of four-well microfluidic chips connected by three different shaped channels (straight, sawtooth, and spiral channels). Each set of channels is fabricated at different depths separated by 200 μm. **(b1–b3)** Zoomed images of the microchannel focused at different depths to highlight the different shaped channels. This structure was fabricated with PDMS as fabrication window. PDMS, polydimethylsiloxane. Color images are available online.

shown in Figure 4b1–b3. It is also worth noting that similar structures are printed using Teflon thin films as fabrication window, as given in Kunwar et al.[18]

Discussion

Recently, a new HLP technology is reported that is capable of printing 3D, multiscale, multimaterial structures in additive and subtractive modes with micrometer resolution in commonly used hydrogels.[18] HLP combines the key advantages of lithography (high-resolution) and 3D printing (quick on-demand fabrication with high design flexibility). Use of the oxygen-permeable film is an essential element in HLP and facilitates the additive printing process by creating a dead zone and the subtractive printing process by creating an ablation z-range, as explained below.[18]

When light-based digital projection lithography is performed above an oxygen-permeable film, a dead zone (also known as a crosslinking inhibition zone) is formed as oxygen inhibits photocrosslinking by quenching the excited photoinitiator or by forming peroxide when it combines with a free radical.[17,21,22] Dead zone prevents the adhesion of newly crosslinked layers to the fabrication window and defines the relationship between fabrication speed and part resolution in the additive mode.[17,18,23] In this article, we estimated the dead zone for the commonly available low-cost oxygen-permeable films, namely PDMS-1 films (600 μm thick), PDMS-2 film (spin-coated PDMS thin film (40 μm thick) on glass coverslip), and PU-film (breathe-easy polyurethane film (20 μm thick) laminated on glass coverslip), and compared the result with the commonly used exclusive and expensive Teflon thin films. For the laser dosages used in this work, the dead zone thickness varied from 8 to 97 μm for Teflon and from 48 to 151 μm for PDMS-1 film. For the same laser doses, the dead zone thickness ranges obtained for the PDMS-2 film and PU film were ~6.4–114 and 4–45 μm, respectively. Due to the presence of the dead zone, the photocrosslinked part is continuously drawn out of the sample holder and the advancing part creates suction forces that

constantly draw liquid resin into the fabrication area.[17] This facilities continuous and fast printing of the structures,[17,18,24] unlike the traditional stereolithography approach that is a sequential and slow process of printing.[25,26] For instance, in this work, a printing speed of 1.44 m/h was obtained using PDMS-1, PDMS-2, and Teflon films, and a printing speed of 0.7 m/h was achieved with PU films. However, the speed of fabrication is limited to a few millimeters per hour in the case of conventional stereolithography.[24]

The ablation z-range for subtractive mode of printing is also fundamental to the HLP process.[18] Within the ablation z-range, material can be reliably removed using laser-based ablation and is important to determine the exact location of laser focus during the subtractive mode of fabrication.[18] Due to light absorption and scattering, the two-photon ablation process is limited to a certain depth and this defines the upper end of the ablation z-range.[18,27] The region just above the dead-zone within the crosslinked hydrogel layer marks the lower end of the ''ablation z-range.''[18] The ''ablation z-range'' for the PDMS-1 film and Teflon film was ~40–70 and ~30–80 μm, respectively, when a crosslinking laser power of 200 mW and an exposure time of 20 s were used. These two films were considered suitable for the subtractive mode of fabrication. The ''ablation z-range'' for PDMS-2 and PU films was small (20–40 μm for PDMS-2 and 20–30 μm for PU film) and this results in unwanted crosslinking with bubble formation within the dead zone during subtractive ablation. Hence, these two films are only considered suitable for the additive mode of HLP fabrication.

Conclusion

In conclusion, we have studied and characterized different oxygen-permeable films with reference to additive and subtractive laser printing. The oxygen inhibition zone also known as dead zone created by the presence of oxygen is measured for different laser doses, that we believe is useful for most of the additive projection-based continuous printing. We also estimated the ''ablation z-range,'' which is of utmost

importance for the subtractive mode of fabrication. Based on the results, it is considered that the oxygen-permeable PDMS thin film (600 μm) is suitable for both additive and subtractive modes of fabrication and can fully replace Teflon film, whereas the spin-coated PDMS and breathe-easy PU films are mostly appropriate for the additive mode of fabrication.

Author Disclosure Statement

No competing financial interests exist.

Funding Information

References

1. He Y, Wu Y, Fu J, *et al.* Developments of 3D printing microfluidics and applications in chemistry and biology: A review. Electroanalysis 2016;78:1658–1678.
2. Abdulhameed O, Al-ahmari A, Ameen W, *et al.* Additive manufacturing: Challenges, trends, and applications. Adv Mech Eng 2019;11:1–27.
3. Gul JZ, Sajid M, Rehman MM, *et al.* 3D printing for soft robotics—A review. Sci Technol Adv Mater 2018;19:243–262.
4. Placone JK, Engler A. Recent advances in extrusion-based 3D printing for biomedical applications. Adv Healthc Mater 2018;7;1701161.
5. Hsieh YK, Chen SC, Huang WL, *et al.* Direct micromachining of microfluidic channels on biodegradable materials using laser ablation. Polymers 2017;9:242.
6. Lin C-Y, Li P-K, Cheng LC, *et al.* High-throughput multiphoton-induced three-dimensional ablation and imaging for biotissues. Biomed Opt Express 2015;6:491–499.
7. Xiong W, Zhou YS, He XN, *et al.* Simultaneous additive and subtractive three-dimensional nanofabrication using integrated two-photon polymerization and multiphoton ablation. Light Sci Appl 2012;1:e6.
8. Rogers JA, Nuzzo RG. Recent progress in soft lithography. Material Today 2005;8:50–56.
9. Gamo K. Focused ion beam lithography. Nucl Instrum Methods Phys Res B 1992;65:40.
10. Vieu C, Carcenac F, Pepin A, *et al.* Electron beam lithography: Resolution limits and applications. Appl Surf Sci 2000;164:111–117.
11. Gattass RR, Mazur E. Femtosecond laser micromachining in transparent materials. Nat Photonics 2008;2:219–225.
12. Wong KV, Hernandez A. A review of additive manufacturing. ISRN Mech Eng 2012;208760.
13. Xiong Z, Liu H, Tan X, *et al.* Diffraction analysis of digital micromirror device in maskless photolithography system. Journal of micro/nanolithography. J Micro/Nanolithogr MEMS MOEMS 2014;13:043016.
14. Xiong Z, Li H, Kunwar P, *et al.* Femtosecond laser induced densification within cell-laden hydrogels results in cellular alignment. Biofabrication 2019;11:035005.
15. Selimis A, Mironov V, Farsari M. Direct laser writing: Principles and materials for scaffold 3D printing. Microelectron Eng 2014;132:83–89.
16. Kunwar P, Hassinen J, Bautista G, *et al.* Direct laser writing of photostable fluorescent silver nanoclusters in polymer films. ACS Nano 2014;8:11165–11171.
17. Tumbleston JR, Shirvanyants D, Ermoshkin N, *et al.* Continuous liquid interface production of 3D objects. Science 2015;347:1349–1352.
18. Kunwar P, Xiong Z, Zhu Y, *et al.* Hybrid laser printing of 3D, multiscale, multimaterial hydrogel structures. Adv Opt Mater 2019;1900656.
19. Fairbanks BD, Schwartz MP, Bowman CN, *et al.* Photo-initiated polymerization of PEG-diacrylate with lithium phenyl-2,4,6-trimethylbenzoylphosphinate: Polymerization rate and cytocompatibility. Biomaterials 2009;30:6702–6707.
20. Sarig-nadir O, Livnat N, Zajdman R, *et al.* Laser photo-ablation of guidance microchannels into hydrogels directs cell growth in three dimensions. Biophys J 2009;96:4743–4752.
21. Ligon SC, Husár B, Wutzel H, *et al.* Strategies to reduce oxygen inhibition in photoinduced polymerization. Chem Rev 2014;114;557–589.
22. Yagci Y, Jockusch S, Turro NJ. Photoinitiated polymerization: Advances, challenges, and opportunities. Macromolecules 2010;43;6245–6260.
23. Manapat JZ, Chen Q, Ye P, *et al.* 3D printing of polymer nanocomposites via stereolithography. Macromol Mater Eng 2017;302;1600553.
24. Kunwar P, Jannini AVS, Xiong Z, *et al.* High-resolution 3D printing of stretchable hydrogel structures using optical projection lithography. ACS Appl Mater Interfaces 2020;12:1640–1649.
25. Gibson I, Rosen DW, Stucker B, *et al.* Additive Manufacturing Technologies: Rapid Prototyping to Direct Digital Manufacturing. New York, Springer, 2010.
26. Jacobs PF. Rapid Prototyping & Manufacturing: Fundamentals of StereoLithography. New York, McGraw-Hill, 1993.
27. Pradhan S, Keller K, Sperduto JL, *et al.* Fundamentals of laser-based hydrogel degradation and applications in cell and tissue engineering. Adv Healthc Mater 2017;6:1700681.

Address correspondence to:
Pranav Soman
Department of Biomedical and Chemical Engineering
Syracuse University
318 Bowne hall
Syracuse, NY 13244
USA

E-mail: psoman@syr.edu